

## Impurity-Assisted Tunneling Magnetoresistance under a Weak Magnetic Field

Oihana Txoperena,<sup>1</sup> Yang Song,<sup>2</sup> Lan Qing,<sup>3</sup> Marco Gobbi,<sup>1,4</sup> Luis E. Hueso,<sup>1,5</sup> Hanan Dery,<sup>2,3</sup> and Fèlix Casanova<sup>1,5,\*</sup>

<sup>1</sup>CIC nanoGUNE, 20018 Donostia-San Sebastian, Basque Country, Spain

<sup>2</sup>Department of Electrical and Computer Engineering, University of Rochester, Rochester, New York 14627, USA

<sup>3</sup>Department of Physics and Astronomy, University of Rochester, Rochester, New York 14627, USA

<sup>4</sup>Université de Strasbourg, Institut de Science et d'Ingénierie Supramoléculaires (I.S.I.S.), 67083 Strasbourg, France

<sup>5</sup>IKERBASQUE, Basque Foundation for Science, 48011 Bilbao, Basque Country, Spain

(Received 2 April 2014; published 2 October 2014)

Injection of spins into semiconductors is essential for the integration of the spin functionality into conventional electronics. Insulating layers are often inserted between ferromagnetic metals and semiconductors for obtaining an efficient spin injection, and it is therefore crucial to distinguish between signatures of electrical spin injection and impurity-driven effects in the tunnel barrier. Here we demonstrate an impurity-assisted tunneling magnetoresistance effect in nonmagnetic-insulator-nonmagnetic and ferromagnetic-insulator-nonmagnetic tunnel barriers. In both cases, the effect reflects on-off switching of the tunneling current through impurity channels by the external magnetic field. The reported effect is universal for any impurity-assisted tunneling process and provides an alternative interpretation to a widely used technique that employs the same ferromagnetic electrode to inject and detect spin accumulation.

DOI: 10.1103/PhysRevLett.113.146601

PACS numbers: 72.25.Dc, 72.25.Hg, 73.40.Gk, 75.47.-m

For the realization of semiconductor spintronic devices [1–8], the conductivity mismatch problem [9–12] and the difficulty of manipulating semiconductors at the nanoscale are the main issues delaying the progress of this research field. Employing the so-called three-terminal (3T) setup where a single ferromagnetic-insulator contact is used for both injection and detection of spin-polarized currents was a big step towards this purpose [13]. Because of the simplicity of the micron-sized structures employed, this setup has gained popularity in semiconductor spintronics [13–23]. The Lorentzian-shaped magnetoresistance (MR) effect measured in 3T-semiconductor devices has been often attributed to spin injection on account of the resemblance to the celebrated Hanle effect in optical spin injection experiments [24]. However, it has been increasingly realized that the MR reported depends much on the tunneling process and too little on the semiconductor [13–23]. Furthermore, the typical junction working conditions employed for these measurements, with bias voltage settings much larger than the Zeeman energy, render the signal detection prone to subtle effects driven by impurities embedded in the tunnel barrier [14,25].

In this Letter, we elucidate the physics behind such experiments by focusing on the tunnel barrier. Accordingly, our devices render a compact geometry with an aluminum-oxide tunnel barrier created between metallic electrodes,  $M_1/\text{AlO}_x/M_2$ , as sketched in Fig. 1(a). The  $M_1/\text{AlO}_x/M_2$  devices were fabricated *in situ* in a UHV electron-beam evaporation chamber with integrated shadow masks. The base pressure of the chamber is below  $10^{-9}$  mbar. The thickness of the top and bottom metallic electrodes,  $M_1$  and  $M_2$ , ranged between 10 nm and 15 nm. To decisively probe

the role of impurities in the oxide, a series of devices were fabricated with (1)  $\text{O}_2$  plasma exposure at  $10^{-1}$  mbar at a power ranging from around 24 to 40 W for 120 seconds to 210 seconds to minimize the impurity density, or (2)  $n$ -step ( $n$  from 2 to 5) deposition of a 6 Å Al layer with subsequent oxidation of 20 min at  $10^{-1}$  mbar of  $\text{O}_2$  pressure with no plasma. The latter method allows us to vary the density and locations of impurities [26,27]. The area of the tunnel barrier ranges from  $200 \times 275 \mu\text{m}^2$  to  $375 \times 555 \mu\text{m}^2$ . The junction resistance  $R = V(0)/I$  is measured with the typical four-point sensing configuration shown in Fig. 1(a), and the associated MR signal  $\delta R(B) \equiv [V(B) - V(0)]/I$  is the ratio between the voltage change across the junction and the constant current between the metallic leads when an external magnetic field  $B$  is applied. The total amplitude of  $\delta R(B)$  will be called  $\Delta R$ . By using metallic electrodes, we avoid the complications brought by the Schottky barrier and Fermi-level pinning when using a semiconductor [28], and we are able to establish a direct relation between the measured signals and the tunnel barrier. Moreover, we detect similar MR effects in ferromagnetic-insulator-nonmagnetic (FIN) and nonmagnetic-insulator-nonmagnetic (NIN) devices, and explain both of them by considering the magnetic-field-induced on-off switching of the tunneling current through impurities embedded in the tunnel barrier. This important finding calls for investigation of a novel effect and provides an alternative interpretation to recent 3T spin injection experiments, whose magnetoresistance has been attributed to spin accumulation in nonmagnetic materials. Although we do not rule out spin injection in our FIN devices, spin accumulation is clearly not being measured in our setup,

since the measured signals are many orders of magnitude higher than those expected from the standard theory of spin diffusion and accumulation [26].

Figure 1(b) shows a compilation of the total amplitude of the MR effect multiplied by the total area of the tunnel barrier ( $\Delta R \cdot A$ ) for  $n$ -step tunnel barriers (with  $n = 2, 3, 4$ , and 5) with a variety of metallic electrodes, as well as Al/AIO<sub>x</sub>/Py plasma-oxidized tunnel junctions. For plasma-oxidized AIO<sub>x</sub>,  $M_1 = \text{Al}$  and  $M_2 = \text{Py}$  are used (21 devices in total), and the combinations of  $M_1$  and  $M_2$  metals for  $n$ -step AIO<sub>x</sub> are  $M_1 = \text{Al}$  with  $M_2 = \text{Py}$  (3 devices), with  $M_2 = \text{Al}$  (9 devices), with  $M_2 = \text{Cu}$  (6 devices) and with  $M_2 = \text{Au}$  (4 devices), and  $M_1 = \text{Py}$  combined with  $M_2 = \text{Au}$  (3 devices). Excluding the vast majority of the plasma-oxidized barriers, we find a power law scaling relation between  $\Delta R \cdot A$  and  $R \cdot A$ , with an exponent factor of 1.19 ( $\pm 0.09$ ) [dashed line in Fig. 1(b)]. In the following we focus on the results of two representative impurity-rich NIN (Al/AIO<sub>x</sub>/Al) and FIN (Al/AIO<sub>x</sub>/Py) devices whose tunnel barriers are fabricated by a three-step deposition procedure. Figure 1(c) shows  $\delta R(B)$  of the NIN device modulated by out-of-plane ( $B_{\perp}$ ) and in-plane ( $B_{\parallel}$ ) fields. The full width at half maximum (FWHM) of both curves is 0.065 T and the junction resistance increases with  $B$  regardless of its orientation. We corroborated the isotropy of  $\delta R(B)$  in the NIN device for more magnetic field orientations [29]. Figure 1(d) shows the respective measurements in the FIN device where the FWHM is 0.134 T (0.142 T) and the resistance increases (decreases) when applying an in-plane (out-of-plane) magnetic field. Notably,

the FWHM and  $\Delta R/R$  values in our devices are comparable to the recurring values seen by 3T-FIN devices employing various insulators and nonmagnetic materials [13–20,30,31].

The fact that we observe a nonzero MR signal in NIN devices, where no spin-polarized source is present, indicates that the MR effect is governed by the oxide barriers rather than by non-equilibrium spin accumulation in N. To better understand the underlying tunnel mechanism, Fig. 1(e) shows the temperature dependence of  $R$  in a series of devices with different tunnel barriers. The  $R(T)$  of the plasma-oxidized junction shows a weak temperature dependence, in agreement with direct tunneling transport [32]. In contrast, the data corresponding to  $n$ -step barriers ( $n = 2, 3, 4$ , and 5) show a stronger  $T$  dependence. This dependence can be described by acoustic phonon-assisted tunneling through impurities that dominate the conduction and should follow  $R(T) \propto [\int_0^{\varepsilon_M} d\varepsilon (2n_q(T) + 1)\varepsilon^2]^{\mathcal{N}-1}$ , where  $\mathcal{N}$  is the number of impurities assisting the tunneling event,  $n_q(T) = 1/(e^{\varepsilon/k_B T} - 1)$  is the Bose-Einstein distribution, and  $\varepsilon_M$  is the upper energy of acoustic phonons in the barrier. Figure 1(f) shows that for an  $n$ -step tunnel junction we indeed reproduce the experimental results with  $\varepsilon_M \sim 17$  meV [33] and  $n = \mathcal{N}$ , in agreement with the fabrication method employed. We further support the phonon-assisted tunneling picture by employing the Glazman-Matveev theory [34] to analyze the  $I$ - $V$  curves [29]. Confirmation that the effect is entirely impurity driven comes from the fact that the MR effect is observed in impurity-rich  $n$ -step tunnel barriers while being suppressed in plasma-oxidized barriers where direct tunneling is

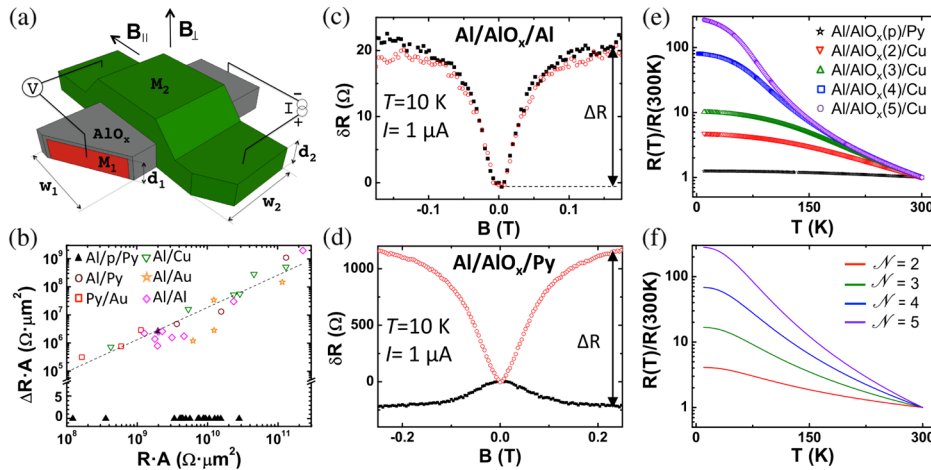


FIG. 1 (color online). Sketch of a tunnel junction, its MR signals and electrical characterization. (a) Scheme of the device and its operation conditions, with the electrode dimensions tagged. (b)  $\Delta R \cdot A$  as a function of the  $R \cdot A$  product for different NIN and FIN devices, measured at 10 K and optimum bias conditions for each device. All the tunnel barriers are  $n$ -step (open symbols), except from the ones labeled as Al/p/Py, which have plasma-oxidized tunnel barriers (solid symbols). Dashed black line is an exponential fit to the data. (c)  $\delta R(B)$  of the NIN device for out-of-plane (solid symbols) and in-plane (empty symbols) fields measured at 10 K and  $1 \mu\text{A}$ , being  $R(0) = 13.7 \text{ k}\Omega$  under these conditions. (d)  $\delta R(B)$  of the FIN device measured at 10 K and  $1 \mu\text{A}$  (injection from  $M_2 = \text{Py}$  into  $M_1 = \text{Al}$ ), with  $R(0) = 158.9 \text{ k}\Omega$ . (e) Normalized  $R(T)$  for a plasma-oxidized barrier, Al/AIO<sub>x</sub>(p)/Py, and  $n$ -step barriers, Al/AIO<sub>x</sub>( $n$ )/Cu, with  $n = 2, 3, 4$ , and 5. All the data have been measured at  $1 \mu\text{A}$ . (f), Theoretical  $R(T)$  curves due to  $\mathcal{N} - 1$  phonon-assisted hops through chains of  $\mathcal{N}$  impurities. The temperature dependence is governed by the sum of phonon emission ( $n_q + 1$ ) and absorption ( $n_q$ ), where  $n_q$  is the Bose-Einstein phonon distribution.

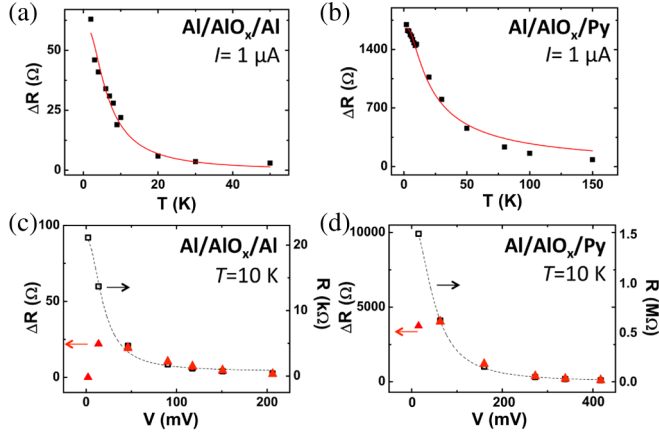


FIG. 2 (color online). Temperature and voltage dependence of the MR amplitude. (a) and (b)  $\Delta R(T)$  measured at  $1 \mu\text{A}$  for the NIN and FIN devices, respectively. The NIN junction bias voltage changes from 14 mV at 2 K to 8 mV at 50 K, and the FIN one from 160 mV at 2 K to 120 mV at 150 K. Red solid lines are Arrhenius fits to the data with activation energies of  $(0.72 \pm 0.07)$  meV for the NIN device and  $(1.55 \pm 0.09)$  meV for the FIN device (see text). (c) and (d) The respective values of  $\Delta R(V)$  and  $R(V)$  measured at 10 K. The signals are symmetric for  $V > 0$  and  $V < 0$ . The black dashed line is a guide to the eye.

dominant [Fig. 1(b)]. The  $T$  and  $V$  dependence of the MR amplitude  $\Delta R$ , displayed in Fig. 2, can be explained in this framework, as will be discussed below. Figures 2(a) and 2(b) show a pronounced decrease of  $\Delta R$  with  $T$  for the NIN and FIN devices, respectively. Figures 2(c) and 2(d) show that, in both NIN and FIN devices,  $\Delta R$  follows a similar voltage dependence as  $R$ , except for a sharp decrease when  $V$  is close to zero. We observe similar voltage dependences for different  $n$ -step barriers [29].

We propose a tunneling mechanism to explain the experimental findings. Using the gained information regarding tunneling across impurity chains in our devices,

we classify impurities with large on-site Coulomb repulsion energy ( $U \gg eV$ ) into type  $A$  and type  $B$  classes. In type  $A$  ( $B$ ), the filling energy for the first (second) electron is within the bias window [35,36]. This simple classification of the energetic levels of the localized states captures the core physics of our experiments. Figure 3(a) shows an example of when both types form an  $A$ - $B$  chain in the tunnel barrier of a NIN junction. When electrons tunnel in the direction from  $A$  to  $B$ , this chain enables on (off) current switching in small (large) external magnetic fields. To understand this effect, we first focus on the steady-state spin configuration in the chain. Once an electron tunnels from the left bank into the type  $A$  impurity, it can be intuitively viewed as an ideal polarized source (“one electron version of a half metal”). Because of Pauli blocking, this electron cannot hop to the second level of the type  $B$  impurity if the first level of the latter is filled with an electron of same spin orientation [see Fig. 3(a)]. The steady-state current across the chain is therefore blocked. This blockade can be lifted when the correlated spin configuration is randomized by spin interactions, which include the spin-orbit coupling [37], hyperfine coupling with the nuclear spin system [38], and spin-spin exchange interactions with unpaired electrons in neighboring impurities [39]. Whichever is the dominant interaction, we can invoke a mean-field approximation and view this interaction as an internal magnetic field at the impurity site that competes with the external field. When the external field is much larger than the internal fields, the type  $A$  and type  $B$  impurities in the chain see similar fields and the current is Pauli blocked as explained before. In the opposite extreme of negligible external field, the blockade is lifted since the correlated spin configuration is violated by spin precession about internal fields that are likely to point in different directions on the  $A$  and  $B$  sites. This behavior is illustrated by Fig. 3(b). Although the  $A$ - $B$  impurity chain is the simplest case that supports magnetic field modulation of

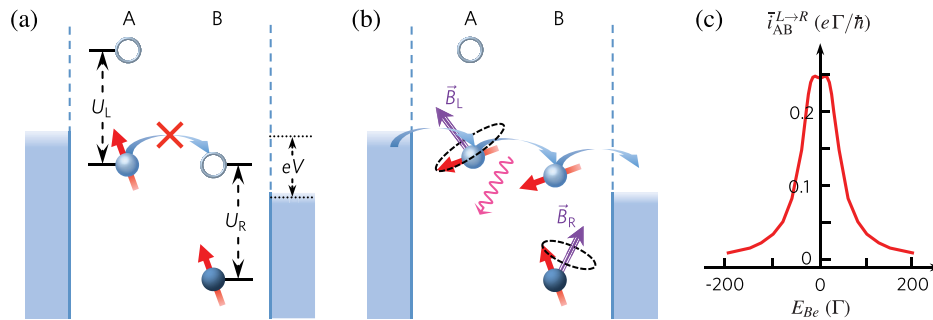


FIG. 3 (color online). Schematics for impurity-assisted MR mechanisms and the theoretical result. (a)  $A$ - $B$  impurity chain in the bias window of a NIN junction. Because of the large on-site Coulomb repulsion ( $U_\ell \gg eV$ ), the current across the chain is Pauli blocked when the electron spins of the lower levels in  $A$  and  $B$  are parallel. (b) The current blocking is lifted when different magnetic fields in  $A$  and  $B$  randomize the correlated spin orientation of the chain (see text). The dominant tunneling process between two impurities is assisted by phonon emission. All the rest of the possible two-impurity chains ( $B$ - $A$ ,  $A$ - $A$ ,  $B$ - $B$ ) do not modulate the current in the NIN junctions [29]. The  $A$ - $B$  impurity chain analyzed in this figure also modulates the current in FIN devices. (c) Theoretical calculation of the current across the  $A$ - $B$  impurity chain as a function of the external magnetic field for a NIN device [see text after Eq. (2)].

the current, similar modulations will also occur in longer chains containing an  $A$ - $B$  sequence.

Next we consider FIN junctions. Because of the magnetization of F, there are two main differences compared to NIN junctions. First, the polarized tunnel current in FIN junctions facilitates partial blocking of the impurity-assisted current already without an external field. In NIN junctions, on the other hand, the current is unblocked without an external field due to the randomized spin configuration induced by the presence of internal fields. As will be explained below, the result is that in FIN junctions the tunnel resistance can either increase (larger blocking) or decrease (weaker blocking) depending on the magnetic field orientation with respect to the magnetization axis of F. The second difference is that chains with at least one  $A$ - $B$  sequence are needed in order to have field modulation in NIN junctions (where the type  $A$  impurity plays the role of “polarizing” the incoming current). In case of FIN junctions, on the other hand, a single impurity is sufficient to block the current. It can be any chain with at least one type  $B$  impurity when electrons flow from F to N (spin injection), or at least one type  $A$  impurity when electrons flow from N to F (spin extraction) [25]. Current blockade is established once the spin in the lower level of the type- $B$ ( $A$ ) impurity is parallel (antiparallel) to the majority spins of F in spin injection (extraction). The blockade is lifted when applying an out-of-plane field whose magnitude is much smaller than the saturation field of F. Spin precession of the electron in the lower level of the type  $B$  ( $A$ ) impurity lifts the blockade since this electron can no longer keep a parallel (antiparallel) spin configuration with the majority spins of F. This physical picture explains the measured reduction in the resistance of the FIN for this field orientation [see Fig. 1(d)]. On the other hand, by applying a field parallel to the magnetization axis of F, the resistance increases since the external field impedes spin precession induced by random internal magnetic fields. Therefore, the current blocked configurations are reinforced: spins in the lower levels of type  $B$  ( $A$ ) impurities are parallel (antiparallel) to the majority spins of F in injection (extraction). Such reinforcement is equivalent to the behavior of NIN junctions under a magnetic field pointing in any direction. The above discussed behavior in FIN junctions explains the measured anisotropy in  $\delta R(B)$  shown in Fig. 1(d). Finally, we emphasize that, details aside, the underlying physics of the MR effect is the same in both FIN and NIN junctions.

To quantify the impurity-assisted tunneling magnetoresistance effect, we describe a toy model based on the tunneling through two-impurity chains by generalizing the Anderson impurity Hamiltonian model to our tunneling case [34]. The steady-state current across the impurity chains is then found by invoking nonequilibrium Green function techniques and deriving master equations in the slave-boson representation [40,41]. The technical details

are given in the Supplemental Material [29]. The steady-state current essentially represents competition between the Zeeman terms, impurity-lead coupling ( $\Gamma_\ell$  where  $\ell = L, R$  denotes left or right impurity-lead pair), and interimpurity coupling ( $\Gamma_{dd}$ ). These coupling terms reflect tunneling rates (via  $\hbar/\Gamma$ ). Solving the master equations for the particular case of the  $A$ - $B$  impurity chain and bias setting described in Fig. 3, we obtain the following steady-state solution for the dominant contribution [29]:

$$i_{AB}^{L \rightarrow R}(\theta) \approx \frac{2e}{\hbar} \left( \frac{1}{\Gamma_L} + \frac{1}{\Gamma_R} - \frac{1}{\Gamma_L + \Gamma_R} + \frac{4}{\Gamma_{dd} \sin^2 \theta} \right)^{-1}. \quad (1)$$

This expression describes the magnetic-field modulated current via an  $A$ - $B$  impurity chain, where the magnetic field dependence is manifested via the angle  $\theta = \theta_R - \theta_L$ . For large enough external field ( $\mathbf{B}_e$ ) the effective fields in the left and right impurities are aligned ( $\mathbf{B}_L \parallel \mathbf{B}_R$ ), and the current is blocked (i.e.,  $\theta \rightarrow 0$  leading to  $i_{AB}^{L \rightarrow R} \rightarrow 0$ ). When  $B_e$  is much smaller than the internal fields, on the other hand,  $\langle \sin^2 \theta \rangle$  is effectively of the order of  $1/2$  after averaging over the distribution of  $\theta$ , and the current can flow. The full expression for  $i_{AB}^{L \rightarrow R}$  is given in Eq. (S3) of the Supplemental Material [29], and in Eq. (1) above we show its simplified form in the limit that the Zeeman energy is larger than the impurity-lead and impurity-impurity couplings ( $\Gamma$ 's). This limit is generally satisfied due to the random distribution of internal fields whose magnitudes and variations can readily exceed those of the weak coupling parameters. In this limit, the FWHM values are determined by the characteristic amplitude of the internal fields. This explains why the stray fields due to the F/I roughness [16] that add to the internal fields in FIN junctions give rise to somewhat larger FWHM values compared to NIN junctions. It also justifies the independence of the measured FWHM values on the thickness of the tunnel barrier. Equation (1) shows a serieslike resistance for the  $A$ - $B$  chain where the negative term,  $-1/(\Gamma_L + \Gamma_R)$ , stems from the coherence between two impurities [29].

We can now recover the measured signal by noting that

$$\frac{\delta R(\mathbf{B}_e)}{R} = N_{AB} \times \frac{\bar{i}_{AB}^{L \rightarrow R}}{I}, \quad (2)$$

where  $N_{AB}$  is the number of  $A$ - $B$  chains with  $U_\ell \gg eV$ , and  $I$  is the total current enabled via tunneling over impurity clusters with various sizes and on-site repulsion  $U$ 's.

All the obtained experimental results are readily understood by applying the above analysis. First, Fig. 3(c) shows a current simulation using Eq. (1) after averaging over the amplitude and orientation of the internal fields. Since the tunneling probability decays exponentially with the barrier thickness, the dominant contribution comes from equidistant impurities for which  $\Gamma_L = \Gamma_R = \Gamma_{dd} = \Gamma$  [36]. Using this equality, we model the internal field in each of

the impurities as an independent normalized Gaussian distribution whose mean and standard deviation are  $20\Gamma$  and  $6\Gamma$ , respectively [29]. We observe that the shape of the simulated curve is in agreement with the Lorentzian shape measured in both NIN and FIN devices [Figs. 1(c) and 1(d)]. Second, we explain the  $\Delta R(T)$  behavior for the NIN and FIN devices. On the one hand, we observe a stronger T dependence of the signal for NIN than for FIN devices [see Figs. 2(a) and 2(b)]. The origin for this behavior is that in NIN devices the blockade is effective when  $U_\ell \gg eV$  for both impurities on the  $A$ - $B$  chain. By contrast, in the FIN devices, it is sufficient to have one such impurity due to the spin polarization of F, rendering  $\Delta R$  less temperature dependent. Using this information,  $\Delta R(T)$  can be fitted by a typical Arrhenius law  $\delta R(T) \propto [1 - \exp(-E_a/k_B T)]^m$  where  $m = 2(1)$  for NIN (FIN) devices. The red lines in Figs. 2(a) and 2(b) show the dependence where the activation energy is  $E_a = 0.72 \pm 0.07$  meV for the NIN device and  $E_a = 1.55 \pm 0.09$  meV for the FIN device. The activation energy  $E_a \sim 1$  meV is associated with the threshold of small impurities to merge into larger clusters resulting in  $U \lesssim eV$  [39]. This scenario is compatible with our devices where apart from isolated impurities, we might also have impurities in close proximity behaving as big clusters as temperature is increased. Third, the decrease of  $\Delta R(V)$  at low bias values [Figs. 2(c) and 2(d)] is due to the vanishing number of  $A$ - $B$  channels within the small bias window. Finally, related to that, the relative signal  $\Delta R/R$  is a result of the small portion of  $A$ - $B$  chains with  $U_\ell \gg eV$  among all cluster chains. The fact that  $\Delta R/R$  is nearly constant comparing all devices, as shown in Fig. 1(b), is in agreement with Eq. (2).

In conclusion, the MR effect shows how the impurity-assisted tunnel resistance can be modulated by a magnetic field when the Zeeman splitting of the impurity spin states is smaller compared to the applied bias voltage. Other impurity-driven effects reported up to date, such as the Kondo effect or Coulomb correlation in resonant tunneling [42–44], appear in the opposite regime at strong magnetic fields. This mechanism therefore promises new possibilities to explore local states in disordered materials or nanostructures. Our analysis puts NIN and FIN junctions on an equal footing, with the physical picture readily generalizable to chains with  $\mathcal{N} \geq 2(1)$  impurities in NIN (FIN) junctions. This novel magnetoresistance effect is general for any impurity-assisted tunneling process regardless of the oxide thickness or materials used. Therefore, the presented work will be used as a benchmark for spin injection experiments to any nonmagnetic material, and specially will redirect research of semiconductor spintronics, with all the implications in such a technologically relevant area.

The authors acknowledge Dr. A. Bedoya-Pinto for fruitful discussions. The work in Spain is supported by the European Union 7th Framework Programme (NMP Project Grant No. 263104-HINTS, Marie Curie Actions

Grant No. 256470-ITAMOSCINOM and the European Research Council Grant No. 257654-SPINTROS), by the Spanish Ministry of Economy under Project No. MAT2012-37638 and by the Basque Government under Project No. PI2011-1. The work in USA is supported by NRI-NSF, NSF, and DTRA Contracts No. DMR-1124601, No. ECCS-1231570, and No. HDTRA1-13-1-0013, respectively.

O. T. and Y. S. contributed equally to this work.

\*Corresponding author.

f.casanova@nanogune.eu

- [1] Y. K. Kato, R. C. Myers, A. C. Gossard, and D. D. Awschalom, *Science* **306**, 1910 (2004).
- [2] S. Murakami, N. Nagaosa, and S.-C. Zhang, *Science* **301**, 1348 (2003).
- [3] I. Žutić, J. Fabian, and S. D. Sarma, *Rev. Mod. Phys.* **76**, 323 (2004).
- [4] H. Dery, P. Dalal, Ł. Cywiński, and L. J. Sham, *Nature (London)* **447**, 573 (2007).
- [5] S. A. Crooker, M. Furis, X. Lou, C. Adelman, D. L. Smith, C. J. Palmstrøm, and P. A. Crowell, *Science* **309**, 2191 (2005).
- [6] I. Appelbaum, B. Huang, and J. Monsma, *Nature (London)* **447**, 295 (2007).
- [7] P. Li, J. Li, L. Qing, H. Dery, and I. Appelbaum, *Phys. Rev. Lett.* **111**, 257204 (2013).
- [8] T. Sasaki, T. Oikawa, M. Shiraishi, Y. Suzuki, and K. Noguchi, *Appl. Phys. Lett.* **98**, 012508 (2011).
- [9] M. Johnson and R. H. Silsbee, *Phys. Rev. B* **35**, 4959 (1987).
- [10] G. Schmidt, D. Ferrand, L. W. Molenkamp, A. T. Filip, and B. J. van Wees, *Phys. Rev. B* **62**, R4790 (2000).
- [11] E. I. Rashba, *Phys. Rev. B* **62**, R16267 (2000).
- [12] A. Fert and H. Jaffrès, *Phys. Rev. B* **64**, 184420 (2001).
- [13] S. P. Dash, S. Sharma, R. S. Patel, M. P. de Jong, and R. Jansen, *Nature (London)* **462**, 491 (2009).
- [14] M. Tran, H. Jaffrès, C. Deranlot, J.-M. George, A. Fert, A. Miard, and A. Lemaître, *Phys. Rev. Lett.* **102**, 036601 (2009).
- [15] C. H. Li, O. M. G. van 't Erve, and B. T. Jonker, *Nat. Commun.* **2**, 245 (2011).
- [16] S. P. Dash, S. Sharma, J. C. Le Breton, J. Peiro, H. Jaffrès, J.-M. George, A. Lemaître, and R. Jansen, *Phys. Rev. B* **84**, 054410 (2011).
- [17] Y. Aoki, M. Kameno, Y. Ando, E. Shikoh, Y. Suzuki, T. Shinjo, M. Shiraishi, T. Sasaki, T. Oikawa, and T. Suzuki, *Phys. Rev. B* **86**, 081201(R) (2012).
- [18] A. Jain *et al.*, *Phys. Rev. Lett.* **109**, 106603 (2012).
- [19] T. Uemura, K. Kondo, J. Fujisawa, K.-I. Matsuda, and M. Yamamoto, *Appl. Phys. Lett.* **101**, 132411 (2012).
- [20] S. Sharma, A. Spiesser, S. P. Dash, S. Iba, S. Watanabe, B. J. van Wees, H. Saito, S. Yuasa, and R. Jansen, *Phys. Rev. B* **89**, 075301 (2014).
- [21] J. Shiogai, M. Ciorga, M. Utz, D. Schuh, M. Kohda, D. Bougeard, T. Nojima, J. Nitta, and D. Weiss, *Phys. Rev. B* **89**, 081307(R) (2014).

- [22] H. N. Tinkey, P. Li, and I. Appelbaum, *Appl. Phys. Lett.* **104**, 232410 (2014).
- [23] A. G. Swartz, S. Harashima, Y. Xie, D. Lu, B. Kim, C. Bell, Y. Hikita, and H. Y. Hwang, *Appl. Phys. Lett.* **105**, 032406 (2014).
- [24] *Optical Orientation*, edited by F. Meier and B. P. Zakharchenya (North-Holland, New York, 1984).
- [25] Y. Song and H. Dery, *Phys. Rev. Lett.* **113**, 047205 (2014).
- [26] O. Txoperena, M. Gobbi, A. Bedoya-Pinto, F. Golmar, X. Sun, L. E. Hueso, and F. Casanova, *Appl. Phys. Lett.* **102**, 192406 (2013).
- [27] W. H. Rippard, A. C. Perrella, F. J. Albert, and R. A. Buhrman, *Phys. Rev. Lett.* **88**, 046805 (2002).
- [28] S. M. Sze, *Physics of Semiconductor Devices* (Wiley, New York, 1981).
- [29] See Supplemental Material at <http://link.aps.org/supplemental/10.1103/PhysRevLett.113.146601> for supporting experiments showing (a) the isotropy of the signal in NIN junctions with respect to the orientation of the magnetic field, (b) analysis of the  $I$ - $V$  curves using the Glazman-Matveev theory for phonon-assisted tunneling, (c) bias dependence of the signal in NIN junctions with 3-step, 4-step and 5-step tunnel barriers. In addition, it includes the Hamiltonian model and resulting master equations along with analytical expressions for the tunnel current. It also includes simulation details for the results of Fig. 3(c), and a quantitative discussion showing the proposed MR effect can elucidate recent experimental results of FIN junctions where N is a semiconductor.
- [30] O. M. J. van 't Erve, A. L. Friedman, E. Cobas, C. H. Li, J. T. Robinson, and B. T. Jonker, *Nat. Nanotechnol.* **7**, 737 (2012).
- [31] W. Han, X. Jiang, A. Kajdos, S.-H. Yang, S. Stemmer, and S. S. P. Parkin, *Nat. Commun.* **4**, 2134 (2013).
- [32] J. J. Åkerman, R. Escudero, C. Leighton, S. Kim, D. A. Rabson, R. Whig Dave, J. M. Slaughter, and I. K. Schuller, *J. Magn. Magn. Mater.* **240**, 86 (2002).
- [33] R. Heid, D. Strauch, and K.-P. Bohnen, *Phys. Rev. B* **61**, 8625 (2000).
- [34] L. I. Glazman and K. A. Matveev, *Zh. Eksp. Teor. Fiz.* **94**, 332 (1988) [*Sov. Phys. JETP* **67**, 1276 (1988)].
- [35] L. I. Glazman and K. A. Matveev, *Pis'ma Zh. Eksp. Teor. Fiz.* **48**, 403 (1988) [*JETP Lett.* **48**, 445 (1988)].
- [36] H. Bahlouli, K. A. Matveev, D. Ephron, and M. R. Beasley, *Phys. Rev. B* **49**, 14496 (1994).
- [37] R. Prioli and J. S. Helman, *Phys. Rev. B* **52**, 7887 (1995).
- [38] M. Boero, A. Pasquarello, J. Sarnthein, and R. Car, *Phys. Rev. Lett.* **78**, 887 (1997).
- [39] J. S. Helman and B. Abeles, *Phys. Rev. Lett.* **37**, 1429 (1976).
- [40] Z. Zou and P. W. Anderson, *Phys. Rev. B* **37**, 627(R) (1988).
- [41] J. C. Le Guillou and E. Ragoucy, *Phys. Rev. B* **52**, 2403 (1995).
- [42] D. Goldhaber-Gordon, H. Shtrikman, D. Mahalu, D. Abusch-Magder, U. Meirav, and M. A. Kastner, *Nature (London)* **391**, 156 (1998).
- [43] D. Ephron, Y. Xu, and M. R. Beasley, *Phys. Rev. Lett.* **69**, 3112 (1992).
- [44] Y. Xu, D. Ephron, and M. R. Beasley, *Phys. Rev. B* **52**, 2843 (1995).